Ship Resistance Prediction by Free-Surface RANS Computations

Rodrigo Azcueta, TU Hamburg-Harburg[1]

1 Numerical method

The turbulent flow around ships including the free surface is computed using the Reynolds-averaged Navier-Stokes equation solver ICCM-Comet. The finite volume method uses control volumes (CVs) with an arbitrary number of faces and allows cell-wise local mesh refinement. Both air and water are considered as a single fluid with variable properties. An additional transport equation for a void fraction of liquid is solved to determine the interface between the two fluids (interface-capturing method). An interface-capturing scheme determines the shape of the free surface. The HRIC discretization scheme for convective fluxes in the void fraction equation is used to ensure the sharpness of the interface, *Demiržić and Muzaferija (1995), Muzaferija and Perić (1998).* The integration in space is of second order, based on midpoint rule integration and linear interpolation. The method is fully implicit and uses quadratic interpolation in time through three time levels. The solution method is of pressure-correction type. The standard k–ε turbulence model with wall function is employed. Picard iterations account for the non-linearity of equations. The linear equation systems are solved by conjugate gradient type solvers. The method is parallelised by domain decomposition in both space and time, *Schreck and Perić (1993), Seidl et al. (1998).*

2 Test cases

Only one half of the hull was considered due to symmetry. Single-block grids were used with CVs smaller at the ship ends, near the wall and the free surface. Grid spacing expanded continuously with factors 1.1 to 1.2 in all directions away from the hull and the waterplane. An elliptical grid generator was used that kept the grid lines nearly orthogonal and spacing between the wall and the first grid line nearly constant, *Cura Hochbaum (1993).*

At the inlet, the velocity of both water and air was set to the hull velocity, and the turbulent parameters were derived from a turbulent intensity of 1% and a turbulent viscosity of the same order as the molecular viscosity. No special treatment of the turbulence model was incorporated for the free surface region. Top, bottom and lateral boundaries were treated as slip walls. At the outlet, extrapolation in stream-wise direction was used, and the hydrostatic pressure was specified according to a prescribed water level. No artificial damping of radiating waves in the far field was applied because the waves dissipate sufficiently due to numerical diffusion in the larger outer cells. As an initial condition in the simulation, the full model speed over the entire computational field was imposed without accelerating the flow from rest. The numerical method was robust enough to cope with this kind of shock, and faster convergence was attained this way.

Experimental C_F values were determined using the ITTC correlation line, and the experimental C_P is determined as $C_T - C_F$.

2.1 Wigley hull

The Wigley hull as a test case is still used due to its simple geometrical form and thus ease in grid generation, and due to the large amount of experimental and computational data against which to compare. A Reynolds number $R_n = 5.95 \cdot 10^6$ and a Froude number $F_n = 0.267$ as in the model test (4 m model) of the Ship Research Institute (SRI), *N.N. (1983)*, were set. Three grids with hexahedral CVs were used, Table I. The computational domain extended 1.0 L ahead of the model, 2.0 L to the side and in the wake, and 1.0 L below and 0.05 L (air layer) above the still water surface.

Perpendicular to the hull (y-direction), the spacing varies for the three grids from $0.0002L$ at the bow to $0.00058L$ at the stern, in an attempt to keep a constant nondimensional wall distance

[1]AB 3-13, Lämmersieth 90, D-22305 Hamburg, rodrigo@schiffbau.uni-hamburg.de

$Y^+ \approx 50$. Table II compares resistance coefficients for the three grids. The computed values depend on the blending factor for the discretization of convective fluxes in the momentum equations and on the nondimensional time step size. Here they were set at 90% central differencing and $\delta t = 0.002$, see next section. Fig.1 shows the wave pattern at steady state, Fig.2 the wave profile on the hull.

Table I: Grids for Wigley: CVs and grid spacing, used computer and CPU time for 5000 time steps or time needed for a particle to travel nearly 42 L

Grid	CVs	CVs in $x \cdot y \cdot z$	Δx	Δz	computer	CPU [hrs]
coarse	$24,000$	$60 \cdot 20 \cdot 20$	$0.01L$	$0.0030L$	pentium 166 (sgi900 1 proc.)	8 (3.5)
medium	$192,000$	$120 \cdot 40 \cdot 40$	$0.005L$	$0.0015L$	pentium 166 (sgi900 8 proc.)	66 (3.9)
fine	$648,000$	$180 \cdot 60 \cdot 60$	$0.004L$	$0.0010L$	sgi900 8 proc.	14

Table II: Resistance coefficients for Wigley hull

Grid	C_F	C_P	C_T	$(C_{T,cfd} - C_{T,exp})/C_{T,exp}$
coarse	$3.29{\cdot}10^{-3}$	$1.10{\cdot}10^{-3}$	$4.39{\cdot}10^{-3}$	5.5%
medium	$3.17{\cdot}10^{-3}$	$1.06{\cdot}10^{-3}$	$4.23{\cdot}10^{-3}$	1.7%
fine	$3.20{\cdot}10^{-3}$	$1.04{\cdot}10^{-3}$	$4.24{\cdot}10^{-3}$	1.9%
exp.	$3.29{\cdot}10^{-3}$	$0.87{\cdot}10^{-3}$	$4.16{\cdot}10^{-3}$	

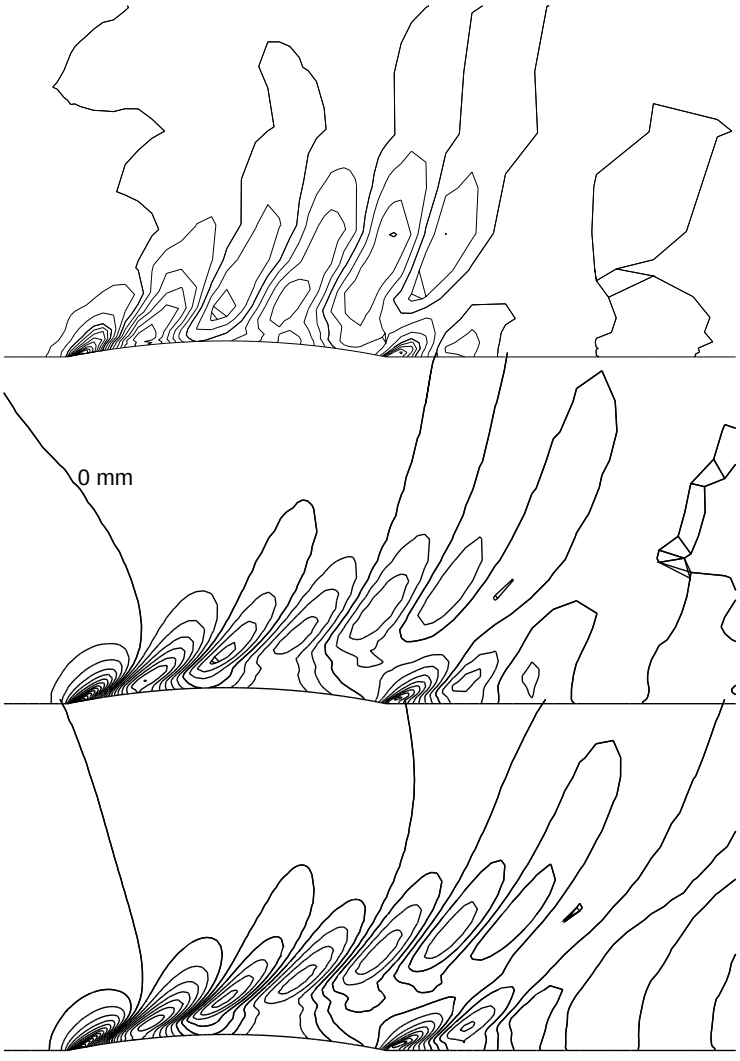

Fig.1: Computed wave pattern around the Wigley hull at $F_n = 0.267$. From top to bottom: coarse, medium and fine grid. Spacing between lines: $0.001L$

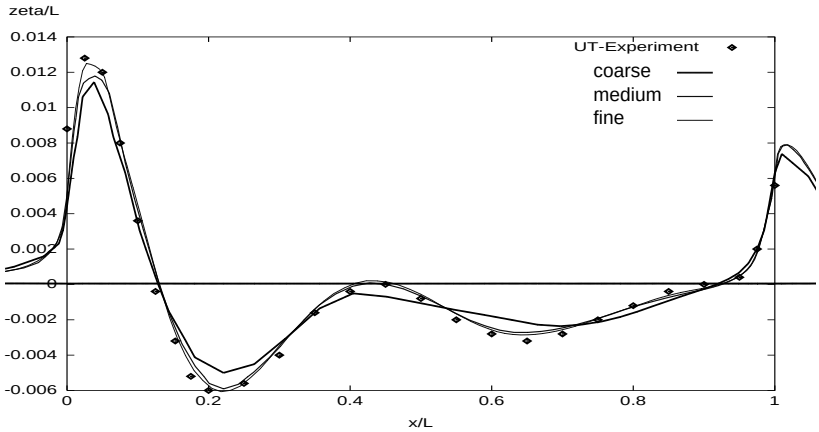

Fig.2: Predicted and measured free surface elevation along the Wigley hull at $F_n = 0.267$ (experiments from the University of Tokyo)

2.2 Series 60 model

The Series 60 with $C_B = 0.6$ was computed at $R_n = 4 \cdot 10^6$ and $F_n = 0.316$. Results are compared to experiments of *Toda et al. (1992)*. Computations were carried out on three numerical grids, Table III.

Mori and Hinatsu (1994) recommend minimum cell sizes to capture the transverse and diverging waves as: $\Delta x < 0.021L$ and $\Delta y < 0.005L$ for $F_n = 0.316$, corresponding to 20 to 30 cells per wave length. The finest grid used satisfies the Δx criterion along the hull (largest cells in the middle of the hull $0.012L$) and up to $0.36L$ behind the stern. The Δy criterion is satisfied up to $0.13L$ from the wall. The computational domain extended 0.75 L ahead of the bow, 1.5 L in the wake and to the side, 1.0 L below and 0.1 L above the design waterline. Table IV compares resistance coefficients. Computational results were obtained using 0.90% central differencing and a $\delta t = 0.0025$.

Both pressure resistance and total resistance coefficients are considerably underestimated. The error decreases with grid refinement. Other towing tank measurements show residual resistance coefficients between $1.8 - 2.0 \cdot 10^{-3}$, *Kajitani (1987)*, which are much closer to computed values. The main explanation for the differences is that computations do not consider the dynamic trim and sinkage of the model. We know from experiments that this can affect the residual resistance by as much as 20%, *Kajitani (1987)*. Fig.3 compares wave patterns. Both measurement and computations were performed in this case at model-fixed condition. The improvement with grid refinement is remarkable only at a certain distance from the model. The wave profile along the hull obtained with the coarse grid shows already a good agreement with subsequent finer grids, Fig.4. The agreement with measured values is not as good as for the Wigley hull.

Table III: Grids for Series 60; cell numbers total, lengthwise, transverse and girthwise; resolution at hull; minimum grid spacings Δx and δy at ship ends, Y^+ averaged at $L/2$; Δz at free surface; used computer and CPU time for 5000 time steps or time needed for a particle to travel nearly 50 L

Grid	CVs	$l \cdot t \cdot g$	at hull	min Δx	Δy (bow/stern)	Y^+	Δz	CPU [h]	computer
coarse	19,456	64·19·16	38·19	$0.0068L$	$0.0022L/0.0064L$	200	$0.0025L$	2.3	sgi900 1 proc.
medium	155,648	128·38·32	78·38	$0.0026L$	$0.0008L/0.0029L$	100	$0.0012L$	8.7	sgi900 4 proc.
fine	1,245,184	256·76·64	156·76	$0.0014L$	$0.0003L/0.0015L$	50	$0.0005L$	41.5	sgi900 8 proc.

Table IV: Resistance coefficients for Series 60

Grid	C_F	C_P	C_T	$(C_{T,cfd} - C_{T,exp})/C_{T,exp}$
coarse	$3.13 \cdot 10^{-3}$	$1.68 \cdot 10^{-3}$	$4.81 \cdot 10^{-3}$	-19%
medium	$3.40 \cdot 10^{-3}$	$1.70 \cdot 10^{-3}$	$5.10 \cdot 10^{-3}$	-14%
fine	$3.53 \cdot 10^{-3}$	$1.72 \cdot 10^{-3}$	$5.25 \cdot 10^{-3}$	-12%
exp.	$3.54 \cdot 10^{-3}$	$2.42 \cdot 10^{-3}$	$5.96 \cdot 10^{-3}$	

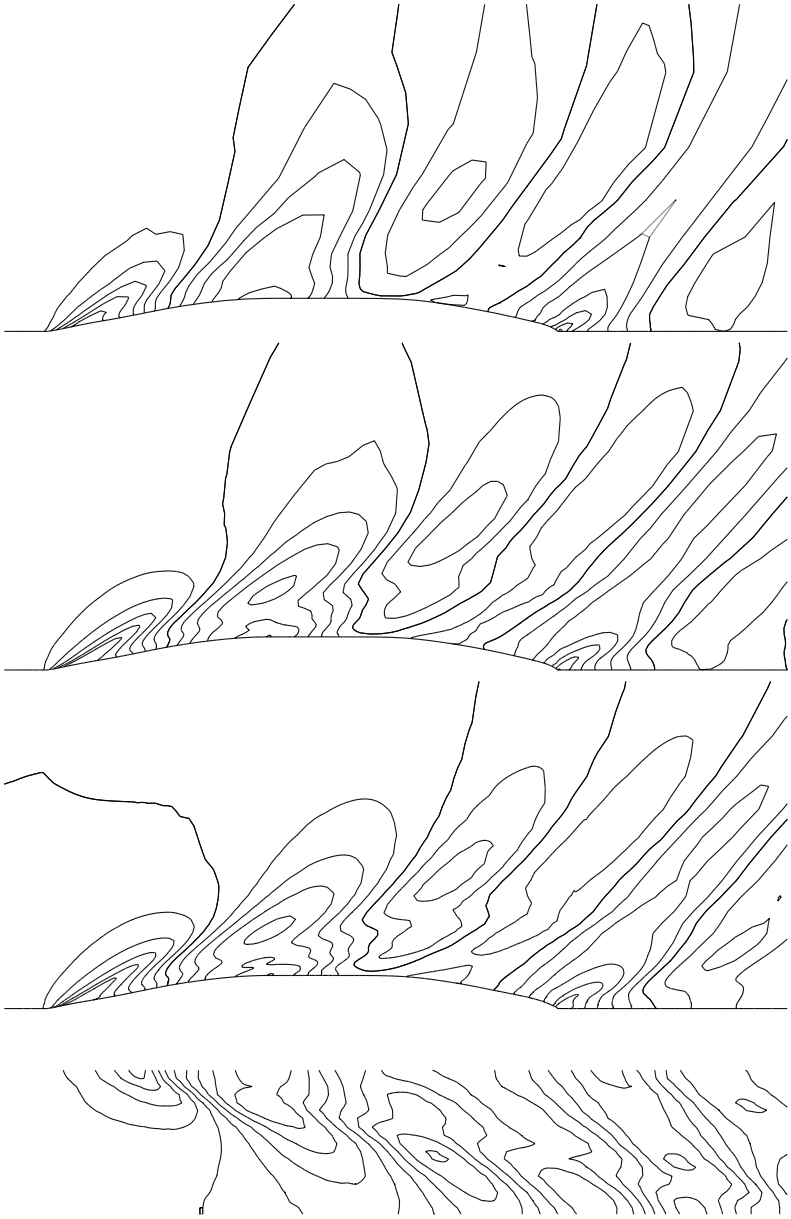

Fig.3: Computed and measured wave patterns around the Series 60 model at $F_n = 0.316$. From top to bottom: coarse, medium, and fine grid and experiments. Spacing between lines $0.0025L$.

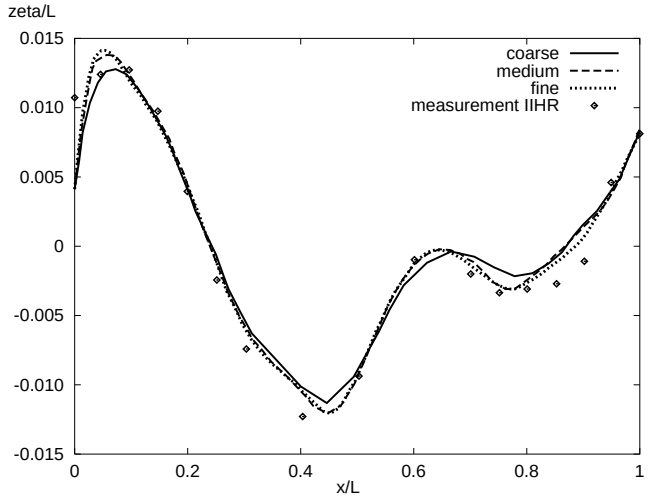

Fig.4: Computed and measured wave profiles along the Series 60 model at $F_n = 0.316$.

3 Dependence of friction resistance on grid quality

Using the standard k–ε turbulence model with wall functions allows lower grid resolution at the wall, thus more CVs at the free surface can be used or higher Reynolds numbers can be computed. However, the model is affected by a strong dependency of the computed friction resistance coefficient on the nondimensional distance Y^+ from the wall to the first cell centre. I cannot confirm the common belief that the range of validity of wall functions extends up to $Y^+ = 500$ or even 1000. Rather an upper limit of $Y^+ = 50$ appears appropriate in my experience (computations at model scale), *Azcueta 2000*.

Fig.5 compares C_F for the Wigley hull to the ITTC value. The computations were performed on seven different coarse grids in which the distance from the wall to the first cell layer was systematically varied. The first grid had a constant distance to the first cell centre along the hull and thus a variable Y^+ of about 400 at $x = L/2$, with higher values at the bow and lower at the stern due to the decelerating flow. The value of C_F on this grid was about 20% lower than the ITTC. The second and third grids had also a variable Y^+ of about 100 and 50, and differed to ITTC by -8% and -2%, respectively. For the fourth grid with a Y^+ value of about 25 the calculation did not converge. The fifth and sixth grids (marked 1 and 2 in Fig.5) had variable distance to the first cell centre and thus an almost constant $Y^+ \approx 100$. To achieve this, the grids were generated by imposing a distance to the first cell centre calculated for each section as a function of the local Reynolds number. The last grid (marked 3 in Fig.5) was similar to the last two, but the spacing to the first cell centre was kept constant in the girth-wise direction as well. This improved the prediction for C_F.

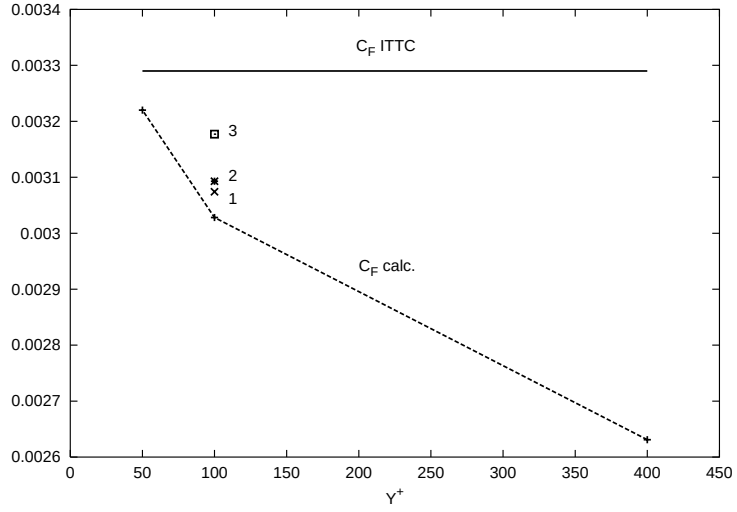

Fig.5: C_F as function of Y^+ for Wigley hull

To investigate the performance of the turbulence model in more detail, calculations with flat plates of finite length were performed. The same strong dependence of C_F on Y^+ could be verified. For these calculations, the Reynolds number was set to $R_n = 4 \cdot 10^6$ with 78 cells along and 40 cells normal to the plate. Two sets of calculations were investigated. In the first one, the spacing from the wall to the first cell centre (constant along the plate length) was varied. From there, the rest of the grid lines expanded evenly to the side boundary situated 2 L away. Thus, the resolution close to the plate also varied. In the second set, the whole grid was kept unchanged but only the first grid line close to the plate was moved to match the different Y^+ values. Both sets of calculations produced similar results. The differences due to varying the resolution by keeping the same Y^+ value were minimal, indicating that the discrepancies are due to a model error and not resolution or discretization errors. In the following, only the results for the first set of calculations will be shown. The Y^+ values, averaged at $x = L/2$, were approximately 400, 200, 100, 50 and 25. Fig.6 compares the computed integral C_F for these cases to the ITTC value. For $Y^+ \approx 400$, the difference to the ITTC value was -32%, while for the last two Y^+ it was about 3.5%.

Fig.7 compares the distribution of the local skin friction coefficient C_f along the plate length for the

different Y^+ values with the theoretical Schlichting line for turbulent flow on a plate, *Schlichting and Gersten (1997)*. For $Y^+ \approx 400$, the calculated and theoretical lines have not much in common. Only if the plate were much longer for the given grid spacing in normal direction, the calculated line would approach the theoretical one. This means that the boundary layer on that grid could not fully develop as it should. Only for the two finest grids is the correspondence to the theoretical line acceptable. The calculated lines run above and below the theoretical line, with errors canceling partially in the integral C_F. An additional calculation was performed with the coarsest grid, where the front 10% of the plate was locally refined until it reached $Y^+ \approx 25$. The improvement in this case was only local (in the refined region) with the boundary layer resolution getting worse immediately behind the refined region (line with the sharp corner by $x = 0.15L$ in Fig.7.

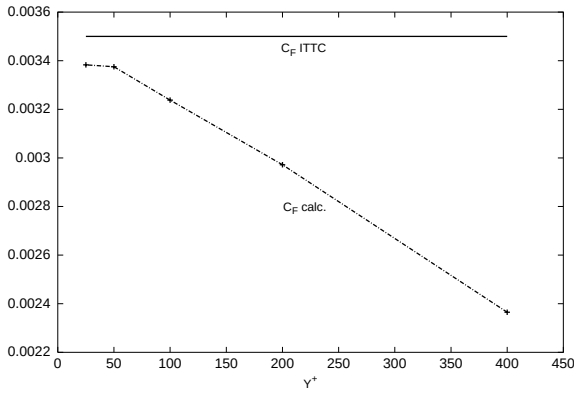

Fig.6: C_F as function of Y^+ for flat plate

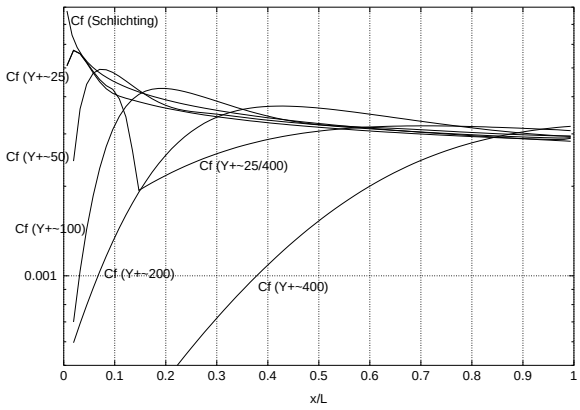

Fig.7: Distribution of local C_f along the plate

Figs.8 and 9 plot nondimensional mean velocity and turbulence kinetic energy profiles for the plate boundary layer. For $Y^+ \approx 400$ at this Reynolds number, the boundary layer is insufficiently resolved with 3 grid points only. For $Y^+ \approx 25$ there are at least 10 grid points inside the boundary layer in the middle of the plate and at the trailing edge. Both velocity profiles are in good agreement with the log-law line.

A similar, qualitatively incorrect distribution of computed local skin friction coefficient was also observed for the flow around the Wigley hull on the $Y^+ \approx 400$ grid. Thus, varying the spacing to the first cell centre along the ship length to account for the decrease of boundary layer thickness towards the bow slightly improves the prediction of friction resistance. This strategy is now my standard practice.

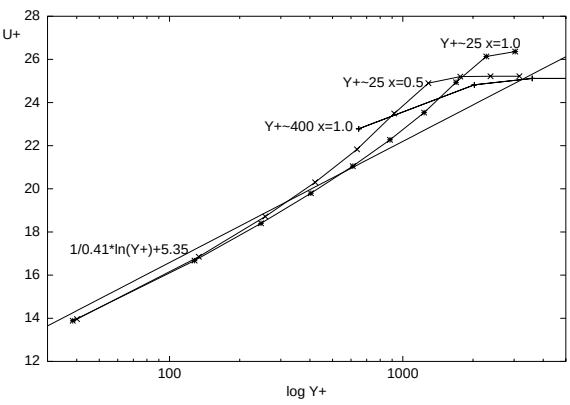

Fig.8: Mean velocity profile compared to log-law. Coarsest grid at trailing edge and finest grid at trailing edge and middle of the plate.

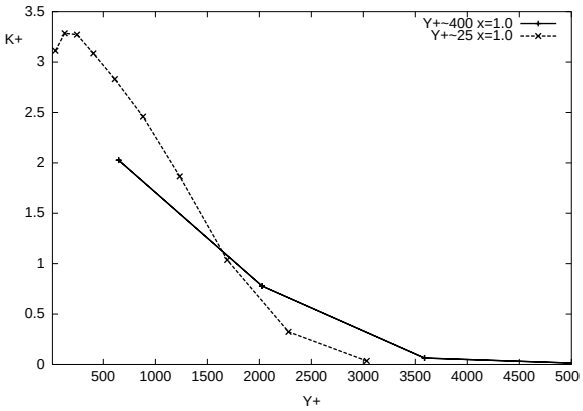

Fig.9: Turbulence kinetic energy profile for coarsest and finest grid at the plate trailing edge.

Another alternative could be to adapt the grid spacing interactively during the computation (re-gridding) to keep a constant Y^+ value or amount of grid points inside the boundary layer. I suggest

to use $Y^+ \approx 50$ or to assure that the first point is within one tenth of the boundary layer thickness, whichever is smaller. This second alternative would yield better results, because Y^+ is much more affected by local form effects (acceleration, deceleration or even separation of flow) than by the normal boundary layer development along a flat plate.

4 Effects of time step size on resistance

The nondimensional time step size δt has to be chosen within certain limits. If it is too large, the integration procedure used (pseudo-time marching) becomes unstable. If it is too small, Rhie & Chow correction will not work properly, the pressure and velocity fields can become decoupled and the calculation oscillates and finally diverges. Integral pressure and friction resistance coefficients depend on the time step size, Figs.10 and 11, which means that several runs have to be calculated to assess a level of uncertainty by varying the time step size, *Azcueta 2000*. The computations were started with a large time step size (i.e. $\delta t = 0.04$), and this was progressively halved until C_P no longer converged. For the Wigley, the variation in C_P for all grids was about 15%. C_F did not vary very much, only about 1%. For the Series 60, the dependence of C_P on δt was between 5% and 10%, and of C_F around 2%. Figs.12 and 13 show C_P and C_F convergence histories with varying δt for the flows around the Wigley hull and Series 60 model, respectively, on the medium grid. While for the Wigley hull there is a clear trend in the effect of reducing δt on C_P, the Series 60 shows no convergence towards any definite value. E.g., for $\delta t = 0.005$ (between 120 s and 140 s), C_P gets definitively smaller than for $\delta t = 0.01$ and $\delta t = 0.0025$. Figs.14 and 15 show the wave pattern and wave profiles (the latter compared with experimental data) for the flow computations around the Wigley hull and Series 60 model on the medium grids, respectively, for four δt values: 0.02, 0.01, 0.005, 0.0025. The wave pattern resolution improves as the time step size is reduced. For the Wigley, δt was halved two more times (0.00125, 0.000625). Then the wave pattern and profile did not change anymore. For the Series 60, reducing δt beyond 0.0025 made the results behave very unstable, Fig.13. There are apparently two sources for this dependency in the solved set of equations. One is the Rhie & Chow correction term, which limits the minimal size of δt for which the results are free from oscillations. The second and dominant one is a Courant number correction in the used discretization scheme for the volume fraction (HRIC). These two δt dependent corrections may interact with each other and it is difficult to separate their effects. More detailed investigations are needed to clarify this point. This dependence of C_P is not a consequence of the pseudo-time marching. Exactly the same results are obtained by performing only one outer iteration per time step or by converging further with many outer iterations within each time step.

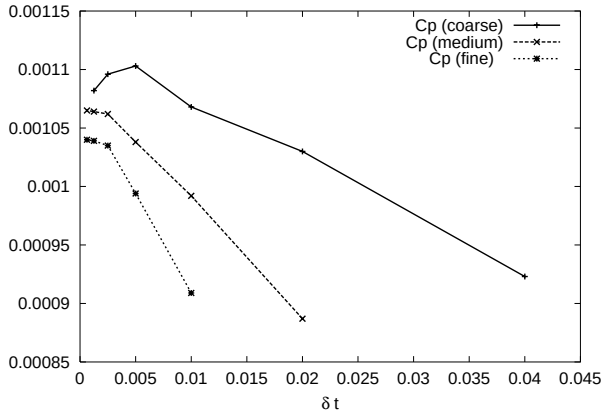

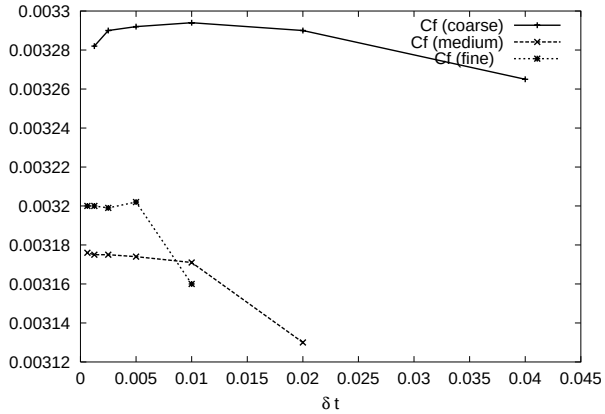

Fig.10: Dependence of the pressure (left) and friction (right) coefficients on the time step size for three different grids for the Wigley hull.

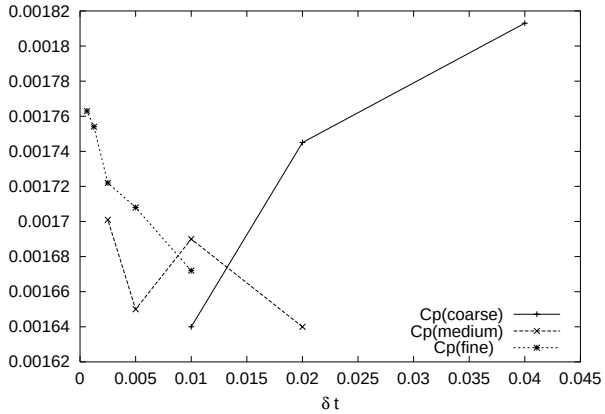

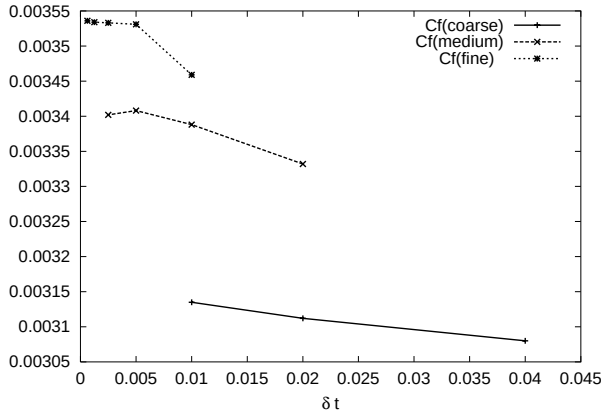

Fig.11: Dependence of the pressure (left) and friction (right) coefficients on the time step size for three different grids for the Series 60 model.

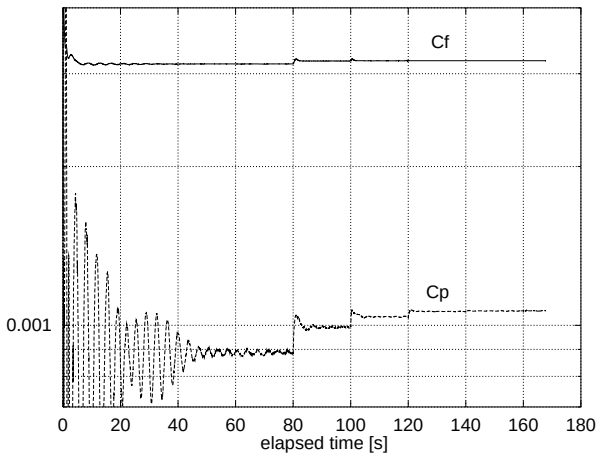

Fig.12: Wigley hull: convergence history of C_P and C_F for varying δt.

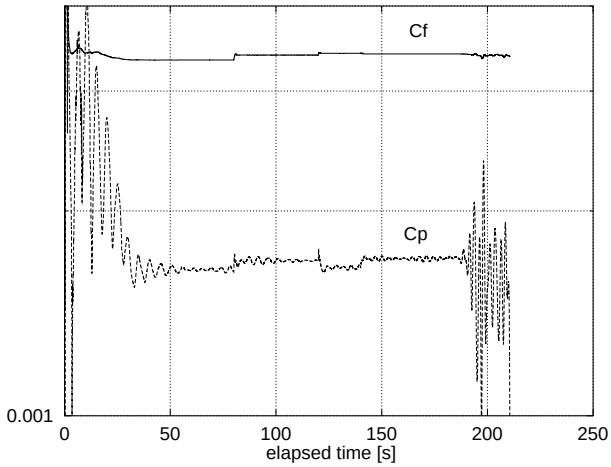

Fig.13: Series 60 model: convergence history of C_P and C_F for varying δt.

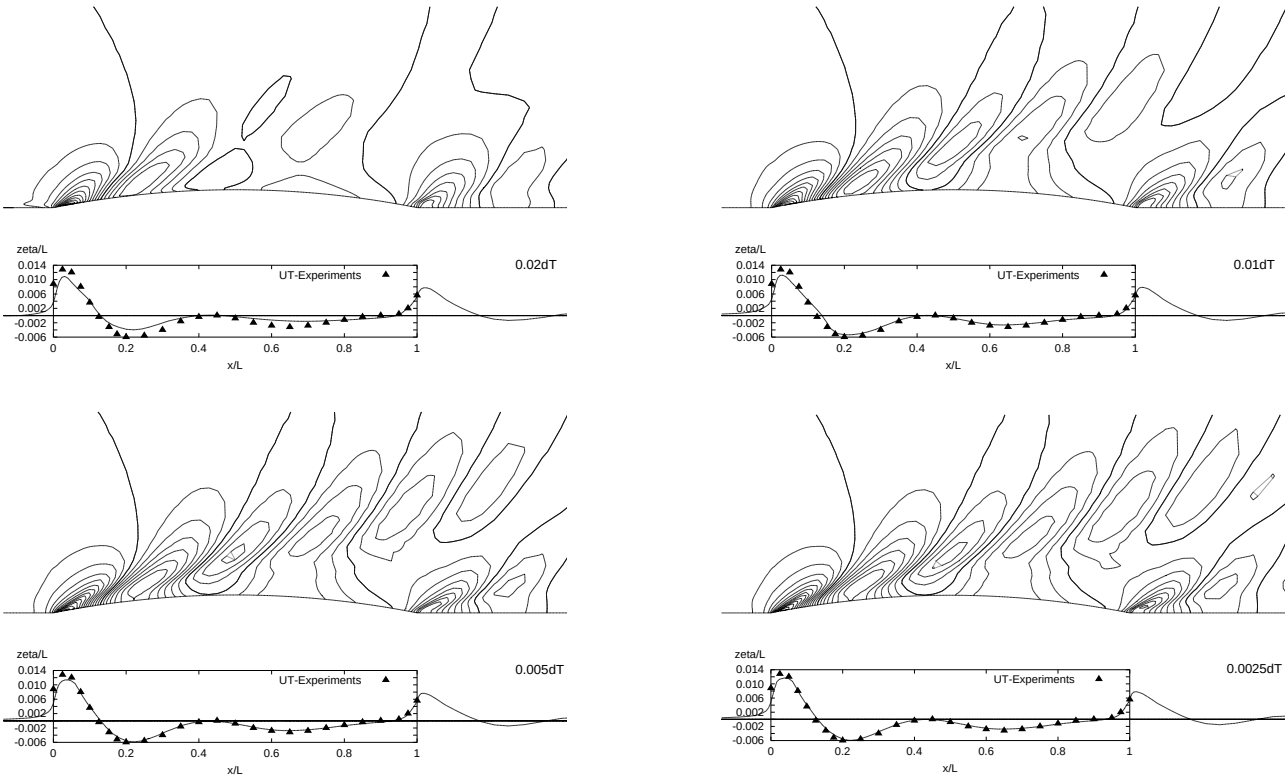

Fig.14: Wave pattern and profile (latter compared with measurements) for the flow around the Wigley hull using four different time steps (medium grid: 192,000 cells).

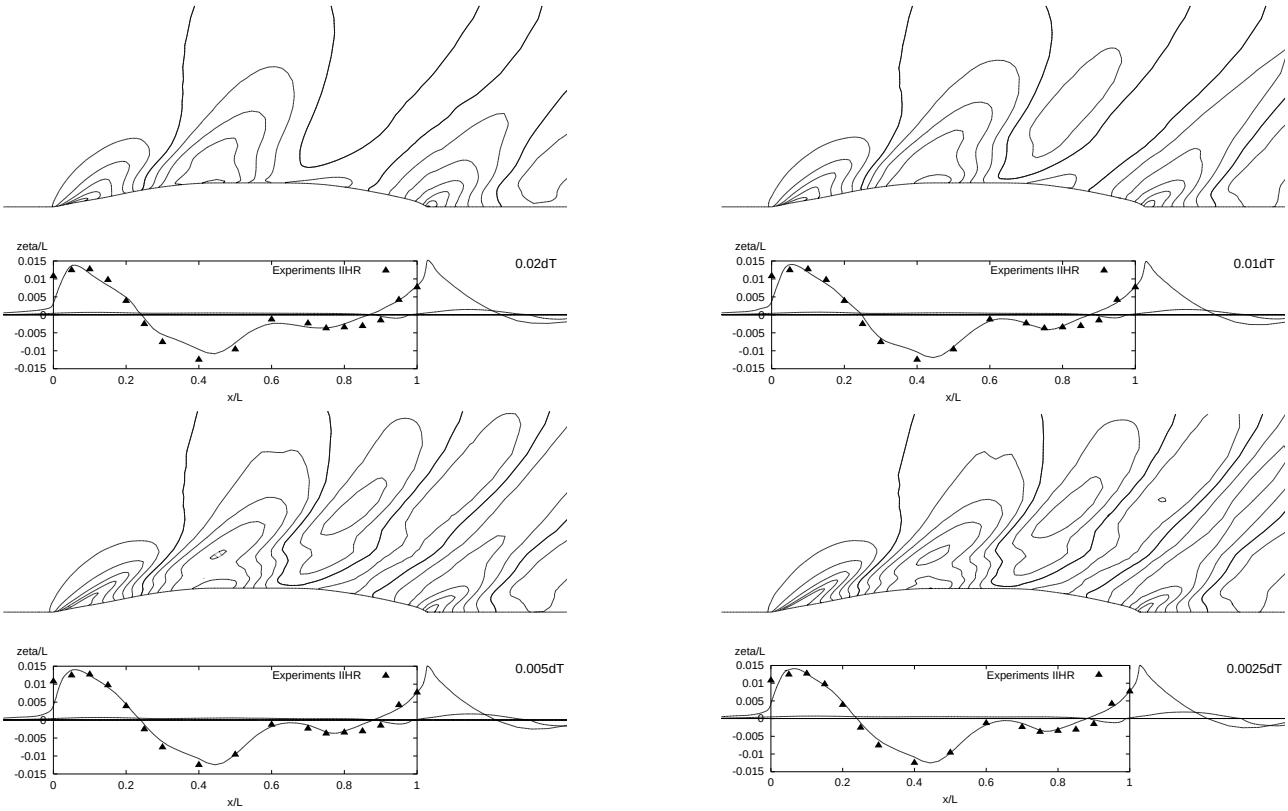

Fig.15: Wave pattern and profile (latter compared with measurements) for the flow around the Series 60 model using four different time steps (medium grid: 155,648 cells).

5 Strategy for best convergence

To try to obtain a steady state free-surface solution with a time marching method usually used for unsteady flows seems not to be the best possible solution. The computational effort penalty is of at least one order of magnitude compared to a steady state flow without free-surface. However, all calculations with free-surface published so far are embedded in time integration procedures. To achieve the best convergence towards the steady state solution of typical free-surface flows using this solver, the following strategy was followed:

- computations were started with the full flow speed, i.e. without accelerating the flow from rest, or alternatively the solution obtained on the next coarser grid was used as initial condition,
- only one iteration per time step was performed throughout the computation,
- the time step size (unique for all CVs) was varied from the largest possible at the beginning to sufficiently small at the end.

In my experience, with only one outer iteration per time step (pseudo-time marching strategy, very similar to the explicit Euler method), the computation converges faster to the steady state solution than by doing more than one iteration per time step but fewer time steps. Furthermore, it is not necessary to satisfy a convergence criterion for outer iterations (of three to four orders of magnitude), because this does not improve the results any further once the steady state solution has been reached.

The size of the time step influences the results. The best results are obtained with the smallest possible time step size, for which convergence is still achieved and the variable fields do not oscillate. The question is then how to reach this solution with a minimal computational effort. Because the pressure coefficient oscillates strongly, it is convenient to try to reduce the oscillations as fast as possible in the first instance. For this purpose it is better to start the computation with the largest possible time step, so that more time units (time that a particle takes to travel one ship length) are calculated with less time steps. Once the amplitude of the oscillation is substantially reduced, one can halve the time step size and continue the computation, and then repeat this procedure so many times until the best possible results are obtained.

Fig.16 shows a typical convergence history for calculations following this strategy. First, 2000 time steps with $\delta t = 0.01$ (40 s simulation time) are performed. The friction coefficient is steady almost from the beginning. The pressure coefficient oscillates, but by 40 s the oscillation is small. After 40 s, the time step size is halved and the computation continues for 1000 time steps up to 50 s. This is repeated three times. This procedure is set before the start of the calculation and runs automatically. Results for each time step size are saved for comparison.

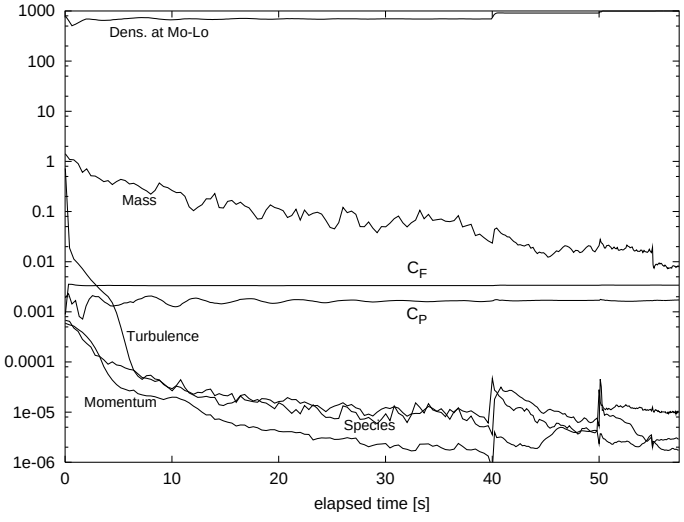

Fig.16: Convergence history of residuals and resistance coefficients for a typical calculation with free surface. The line on top depicts the density at a chosen point near the free surface.

6 Influence of the discretization scheme on pressure resistance

To calculate convective and diffusive fluxes, variable values and their gradients are needed at the cell faces. They have to be interpolated from values at cell centres. The first order upwind differencing scheme (UDS) is numerically diffusive and should be avoided. Second order central differencing scheme (CDS) offers a good compromise among accuracy, simplicity and efficiency, but may produce oscillatory solutions, so it has to be blended with UDS. This blending introduces a possibly significant numerical error.

In order to assess the variation of pressure resistance coefficient for the different discretization schemes resulting from blending UDS with CDS, three different flow cases were systematically studied by varying the mixing ratio of UDS-CDS. The chosen cases were the Wigley hull and Series 60 model using the same grids described earlier (free-surface flows), and a two-dimensional steady flow around a foil section deeply submerged and at zero incidence (no free-surface).

For each flow case and on the three grids, calculations were performed using blending factors varying in 0.1 steps from pure UDS to the maximum possible amount of CDS, typically 90-100% depending on the flow case, grid fineness and quality. In each case, the calculations were carried out for as many time steps as necessary to allow a good average for C_P, after the small oscillations produced by changing the discretization had vanished.

An idealized outcome of the investigation was, Fig.17:

- Results for pure UDS are always too large due to numerical diffusion. They can be too high by a factor two for coarse grids.
- Results for CDS are, although still diffusive, always smaller and closer to reality.
- Between UDS and CDS, the results vary linearly. This has important consequences for the convergence behaviour of the results.
- The slope of the straight lines decreases with grid fineness, and the straight lines cross each other in a unique point, the 'grid independent solution' (G I S).
- By exact extrapolation using the results on the three grids at any constant discretization scheme or blending factor, the same value should be found, which corresponds to the grid independent solution.
- Because the results on any grid behave linearly with varying discretization and the lines cross in a point, the convergence order for this variable is the same and constant at any point of blending between UDS and CDS.

In the actual flow computations, for all cases and grids investigated so far, the results at any blending factor fell on almost straight lines, and these lines crossed each other in a very small region, slightly deviating from the idealised situation described earlier, Figs.18 to 21. If a point of computation did not fall on the straight line, the corresponding computation generally was not accurate enough to average a value for C_P, maybe due to oscillations from reflecting waves, or shock waves created by changing the discretization or starting the computation, or because the amount of CDS was too high so that oscillations in variable fields started to occur.

Results with pure UDS are very diffusive. For coarse grids, a very small C_P values (as in the hydrofoil case) may be 650% too high, and when C_P is most influenced by wave resistance (free-surface ship flows) it may be 80-100% too high. Results on the finer grids were overestimated by about 30% in the ship flow cases. In some cases, by using only 10% less CDS on a fine grid, C_P was as poorly predicted as on a coarser grid. Figs.22 and 23 show how the ratio of UDS-CDS completely change the wave pattern and wave profile for the two free-surface flow cases. With pure UDS the

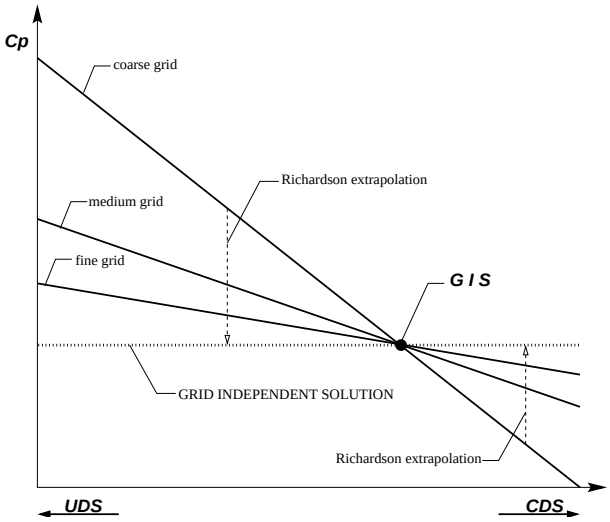

Fig.17: Idealisation of the dependence of computed C_P on the discretization scheme for grids of different fineness.

wave pattern on the finest grid looks worse than with more CDS on the coarsest grid, and this fact is reflected in the C_P values.

Fig.18 shows results from viscous calculations on three grids for the flow around the foil section, as well as the estimated convergence order of the scheme and an estimated grid independent solution using Richardson extrapolation. The estimated order of the scheme at any point of blending varies very little, from 1.02 with pure UDS to 1.17 for 90% CDS. The estimated grid independent solution using Richardson extrapolation vary by 5% from pure UDS to 90% CDS. We can consider as the best extrapolation the one for the largest amount of CDS. The point where the coarse and medium grid lines cross deviates by 6.5% from the extrapolated value at 90% CDS, and that for the medium and fine grid by only 2.5%. The Richardson extrapolation is only an estimate which is as good as the assumptions it makes. Thus we may consider the value where the medium and fine grid lines cross as the most accurate. The value where the medium and coarse grid lines cross may also be an acceptable estimate (it differs from the medium/fine point by only 4%).

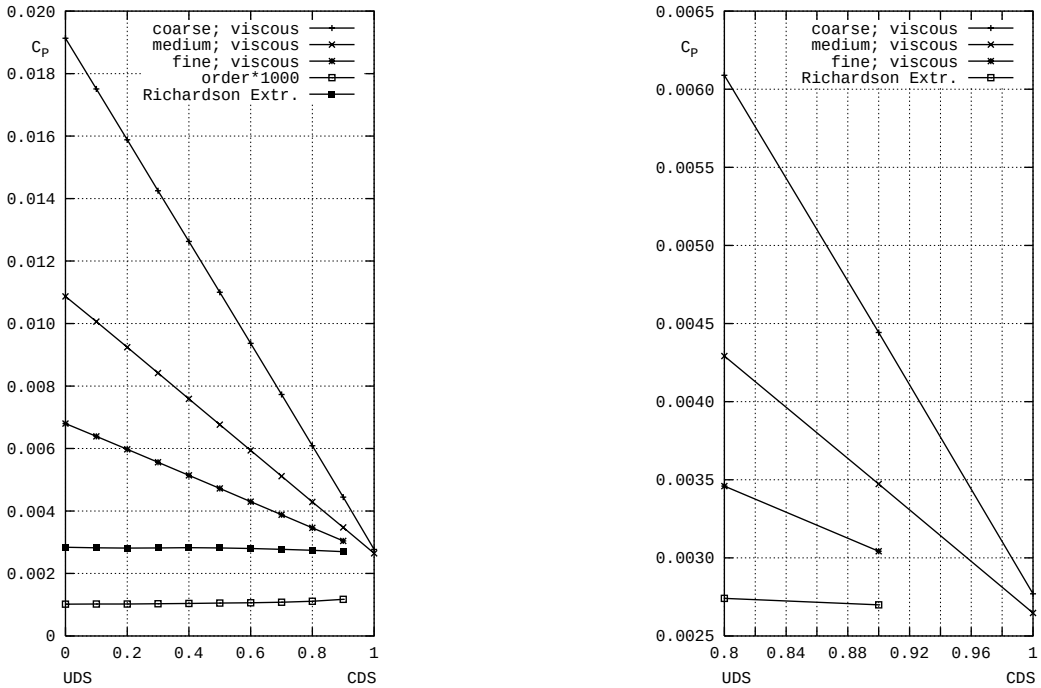

Fig.18: Dependence of C_P on amount of CDS for hydrofoil on three grids (detail on the right).

For the flow around the Wigley model, Fig.19 shows three sets of lines with three lines each. The first set of lines, which lies above the others, corresponds to C_P from the viscous flow calculations including the free-surface deformation, as computed on the three grids presented earlier in this article. The second set of lines, the lowest ones, corresponds to C_P from inviscid (Euler) computations around the double body model. For this purpose, the same grids as for the free-surface viscous calculations were used, replacing the upper block above the water line by a symmetry plane at that height. The C_P value from these inviscid calculations should be nearly zero (no viscosity, no waves, no separation at transom). However, it is not zero but rather large with pure UDS reducing rapidly with more CDS and grid fineness. Where the three lines cross, between 90% and 95% CDS, they are practically very close to zero. This residual value is often considered as a quantity for the discretization error produced in each corresponding grid. If it is further assumed that the numerical errors are almost the same for the viscous and inviscid computations on the same grid, one can subtract the inviscid result from the viscous one and in this way obtain a final result "free" of numerical errors. The last set of lines, the one in the middle, was obtained following this thought. In this case, the resulting lines are almost horizontal and quite close together. One can argue whether this procedure, which is often used, is valid or not, and whether it implies an improvement in resistance prediction. It is commonly believed that the computed pressure resistance contains a component which is always over-predicted due to numerical errors, and the subtraction of this residual C_P leads to an improvement in its prediction.

The three viscous flow lines – or the prolongation of them – cross each other in a small region around 100% CDS. The crossing point between coarse/medium grid lines differs by 3.5% from the crossing point between medium/fine grid lines. By using this type of discretization, any finer grid would deliver a similar C_P value passing near this region. Consequently, a value in this region can be considered as the grid independent solution with an uncertainty of 3.5%. For the Wigley, the range of values where the viscous flow lines cross and that of the purged lines (viscous minus inviscid) is practically the same, indicating that both strategies would deliver the same final result. Unfortunately, the three grids used in this case are not systematically refined (the fine grid has only 4 times more CVs than the medium one), so that the convergence order of the scheme cannot be determined and Richardson extrapolation cannot be applied.

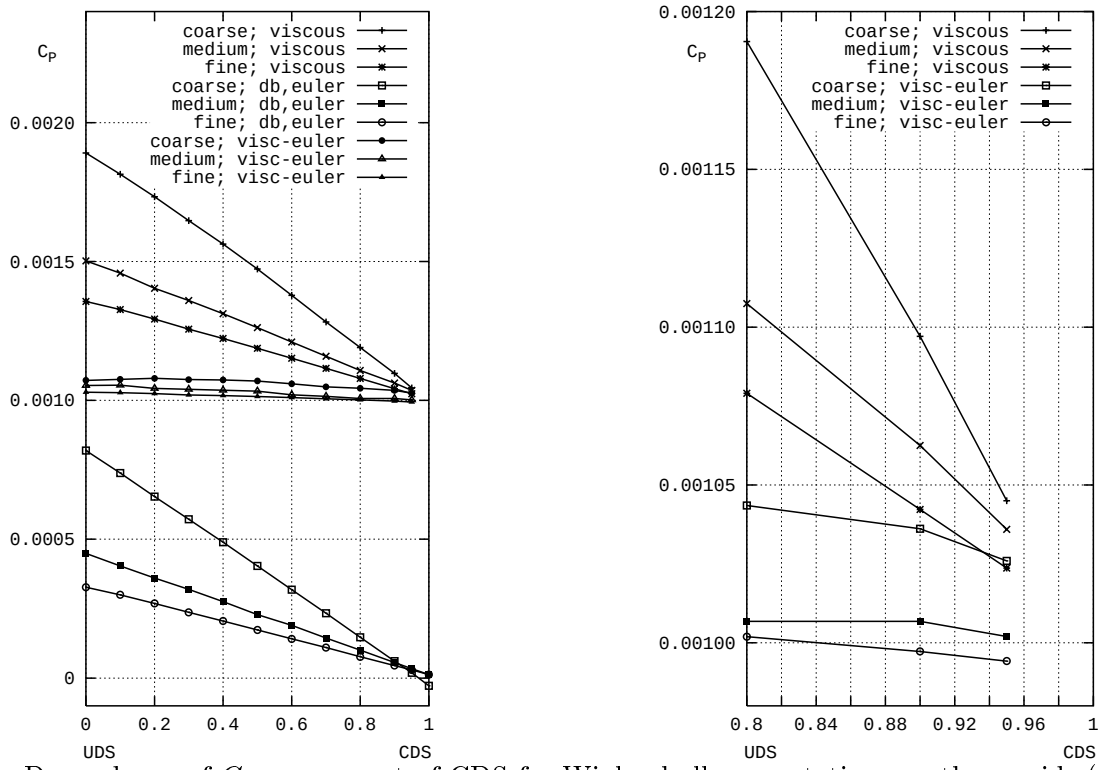

Fig.19: Dependence of C_P on amount of CDS for Wigley hull computations on three grids (detail on the right).

For the Series 60, Fig.20 shows the corresponding results from the viscous and inviscid computations on the three systematically refined grids and the lines corresponding to the difference between these two sets of results. All points of computation lie practically on straight lines. The three viscous lines cross each other at a point between 80% and 90% CDS. The three inviscid (Euler) lines would cross each other close behind 100% CDS where they are basically zero. They are not exactly parallel to the viscous lines, so that the difference between both does not yield horizontal lines (like for the hydrofoil and Wigley) but lines which depend also on the discretization. Thus this strategy is not the best one to find results free of discretization errors. Although for the Wigley one obtains a C_P value by computing on the coarsest grid which deviates by no more of 5% from that on the finest grid, for the Series 60, the difference is larger that 12%, and it may be even larger for other cases.

Fig.21 shows for both the viscous and inviscid calculations the estimated order of convergence for the C_P variable, and an estimate of the grid independent solution using Richardson extrapolation, which in this case can be applied because the grids were systematically refined. In the inviscid case, the convergence order varies from about 0.9 with UDS to 1.7 at 95% CDS. In the viscous case, the convergence order does not improve with more CDS but remains around 1. Richardson extrapolation yields in this case values which lie almost on a horizontal line (variation $< 3.5\%$).

As good an accuracy can be obtained considering the region (here practically a point) where the lines cross each other as the grid independent solution. The great advantage of this proposal is that a comparable accuracy to that from Richardson extrapolation could be obtained by computing on the two coarser grids only. In the Wigley flow case, by considering only the value where the coarse and medium grid lines cross, we had an uncertainty of 3.5%, while in the case of the hydrofoil this was 4%.

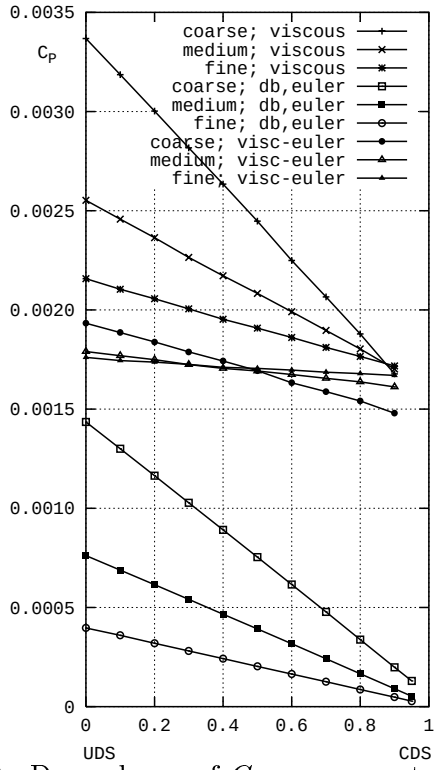

Fig.20: Dependence of C_P on amount of CDS for the Series 60 model. Viscous and Euler computations on three grids and difference between both set of computations.

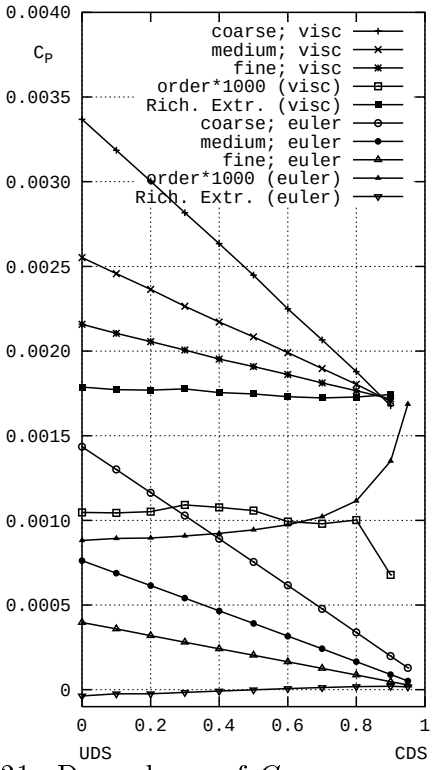

Fig.21: Dependence of C_P on amount of CDS for the Series 60 model. Viscous and Euler computations on three grids, convergence order and Richardson extrapolation.

With a set of three systematically refined grids, the CPU-time needed for computing on the medium grid is at least a factor 10 larger than that on the coarse grid, and that for the fine grid again 10 times larger than that for the medium grid, Table III for the Series 60. To generate and handle a fine grid takes again a lot of additional time. If we were able to compute on coarse and medium grids only

and get an acceptable accuracy, the time saving would be at least a factor 10. It is not necessary to compute at all points of blending. Accurate computations e.g. at 80% and 90% CDS and extrapolating the results suffices, *Azcueta 2000*. It is too early yet to say whether this kind of extrapolation can be of use in practical cases. More flow cases, such as for full ships, and other discretization schemes should be investigated to see if similar trends can be found.

7 Conclusions

Obtaining the right results even with a good code is not easy. Results are very sensitive to grid quality and variation of parameters, and it is difficult to get it right the first time. Many publications show good agreement with experiments, but no detailed analysis of uncertainty. The accuracy requests for resistance predictions are extremely high with a few percent as threshold. Experiments in towing tanks rely upon many assumptions and empirical corrections for the extrapolation to full scale, derived from many decades of experience. Numerical towing tanks have only limited experience. Detailed calculations are needed to try to quantify the sensitivity of results, and find the best extrapolation methods for practical ship design. My work is intended to contribute to this effort.

References

AZCUETA R. (2000), *An analysis of some factors influencing ship resistance prediction based on free-surface flow computations*, Report 605 Arbeitsbereiche Schiffbau TUHH, Hamburg

CURA HOCHBAUM, A. (1993), *Three-dimensional elliptic grid generation with a multigrid method*, 3rd Pan-American Conference of Applied Mechanics, Sao Paulo, pp.267-270

DEMIRDŽIĆ, I.; MUZAFERIJA, S. (1995), *Numerical method for coupled fluid flow, heat transfer and stress analysis using unstructured moving meshes with cells of arbitrary topology*, Comput. Methods Appl. Mech. Eng. 125, pp.235-255

KAJITANI, H. (1987), *A wandering in some ship resistance components and flow*, Ship Technology Research 34, pp.105-131

MORI, K.; HINATSU, M. (1994), *Review of program 1 viscous flow around Series 60 with free-surface*, SRI CFD Workshop, Tokyo, Vol. 2, pp.79-84

MUZAFERIJA, S.; PERIĆ, M. (1998), *Computation of free surface flows using interface-tracking and interface-capturing methods*, Nonlinear Water Wave Interaction, Comp. Mech. Publ.

N.N. (1983), *Cooperative experiments on Wigley parabolic models in Japan*, 17th ITTC Resistance Committee Report, Univ. Tokyo

SCHLICHTING, H.; GERSTEN, K. (1997), *Grenzschicht-Theorie*, Springer

SCHRECK, E. ; PERIĆ, M. (1993), *Computation of fluid flow with a parallel multigrid solver*, Int. J. Numer. Methods in Fluids 16, pp.303-327

SEIDL, V.; MUZAFERIJA, S.; PERIĆ, M. (1998), *Parallel DNS with local grid refinement*, Appl. Scientific Research 59, pp.379-394

TODA, Y.; STERN, F.; LONGO, J. (1992), *Mean-Flow Measurements in the Boundary Layer and Wake Field of a Series 60 $C_b = 0.6$ Ship Model – Part I: Froude Numbers 0.16 and 0.316*, J. Ship Research 36/4

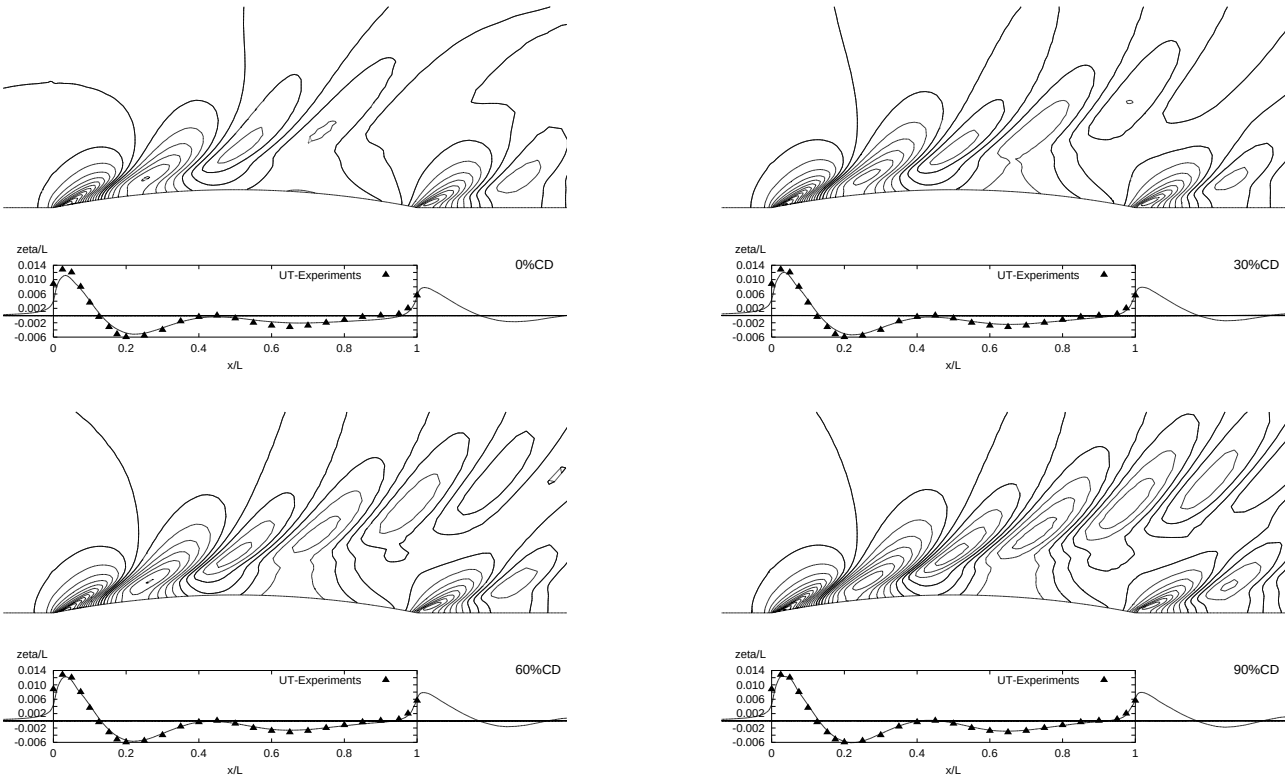

Fig.22: Wave pattern and profile (latter compared with measurements) for the flow around the Wigley hull for varying amount of CDS (fine grid: 648,000 cells).

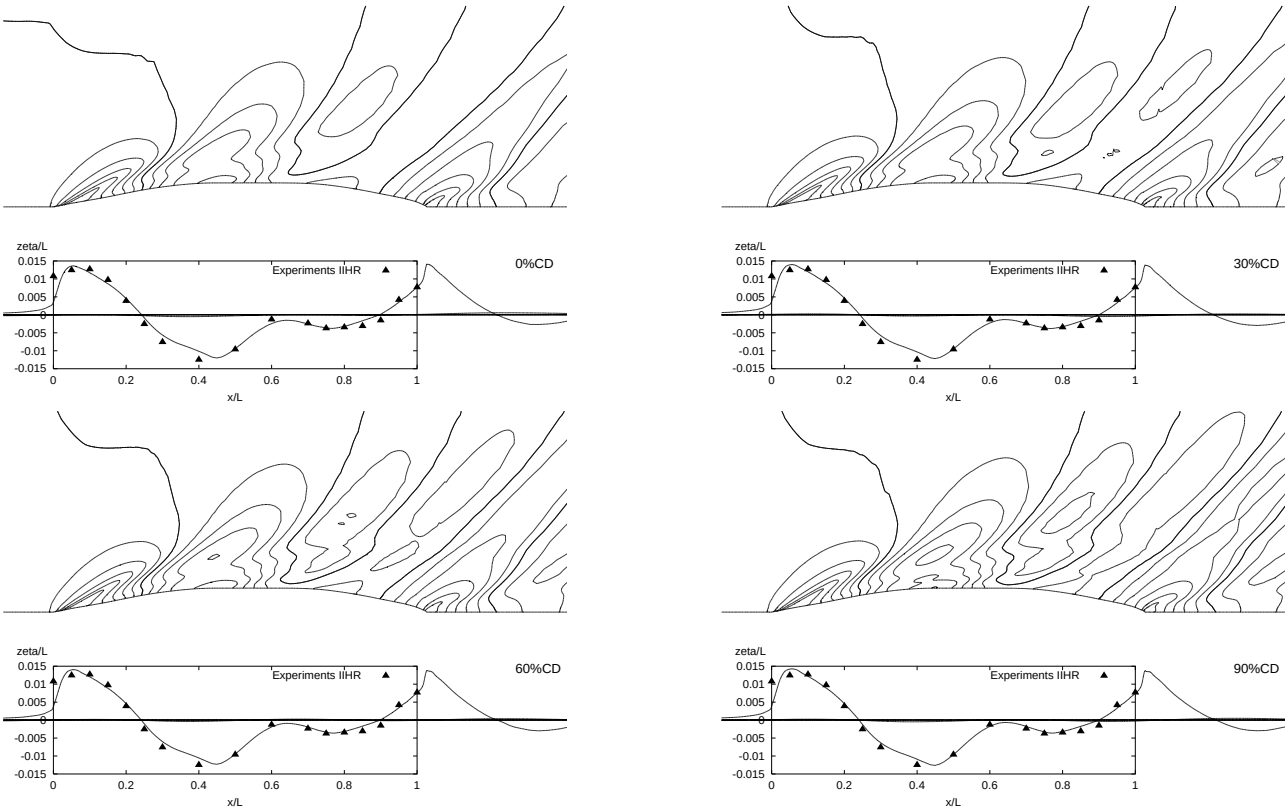

Fig.23: Wave pattern and profile (latter compared with measurements) for the flow around the Series 60 model for varying amount of CDS (fine grid: 1,245,148 cells).